JOURNAL OF SOLID STATE CHEMISTRY 118, 10–19 (1995)

Electronic Properties of Beta-Vanadium Bronzes $Li_xNa_yV_2O_5$ ($0.23 \leq x + y \leq 0.37$) Obtained by the Sol–Gel Process

B. Pecquenard, J. C. Badot, D. Gourier, N. Baffier, and R. Morineau*

Laboratoire de Chimie Appliquée de L'Etat Solide (URA 1466-CNRS), ENSCP, 11 rue P. et M. Curie, 75231 Paris Cédex 05, France; and
**Laboratoire de Chimie de la Matière Condensée (URA 1466-CNRS), UPMC, 4 place Jussieu, 75005 Paris, France*

Received June 30, 1994; in revised form December 27, 1994; accepted January 6, 1995

Vanadium bronzes β-$Li_xNa_yV_2O_5$ ($0.23 \leq x + y \leq 0.37$) have been synthesized by the sol–gel process. These compounds exhibit the monoclinic structure of compounds of the same composition prepared by solid state reaction, but they are obtained as thin layers with a highly preferred orientation. Studies of these compounds by magnetic susceptibility, electron paramagnetic resonance, and electrical conductivity measurements are presented. It is demonstrated from magnetic susceptibility and EPR linewidth that the bipolaron model describes accurately the electronic properties of the lithium and mixed lithium/sodium bronzes synthesized by the sol–gel process. Dc-conductivity measurements between 15 and 300 K show that the bronze conductivities are anisotropic and depend on the nature of the exchanged ion. More complete study on $Li_{0.23}V_2O_5$, including ac-conductivity and impedance measurements from 10 Hz to 10 GHz, gives a good correlation between all the experimental techniques described in this paper.

INTRODUCTION

Monoclinic sodium vanadium bronzes (β-phase) have been recently obtained by the sol–gel process (1). This original route allows one to prepare materials with new morphologies, such as fibers or films with enhanced anisotropy and chemical reactivity (2). The consequence is an easier electrochemical diffusion of lithium in $Na_{0.33}V_2O_5$ bronze obtained by the sol–gel process, indicating that this compound is a promising rechargeable cathodic material (3). It was thus interesting to investigate the electronic properties of the sol–gel compound in order to determine if the difference between the electrochemical behaviors of the sol–gel and classical bronzes could be due to different electronic properties. We have thus studied the electronic properties of the sol–gel $Na_{0.33}V_2O_5$ compound, which were compared with those of the same material obtained by solid state reaction (4).

The structure of β-$Na_{0.33}V_2O_5$ synthesized by solid state reaction has been first resolved by Wadsley (5). The compounds β-$Na_{0.33}V_2O_5$ synthesized by solid state reaction and by the sol–gel process have the same β-monoclinic structure, which is shown in Fig. 1. Three vanadium sites exist in this tunnel structure: octahedral V_1 and V_2 sites and the trigonal bipyramid V_3 site. Each tunnel contains two interstitial equivalent sites labeled M_1 and M_1', in which the alkaline ions are equally distributed. The structure of the β-$Li_xV_2O_5$ with $x = 0.30$ has been studied by Galy *et al.* (6), who showed that this structure is isotypical with the structure of β-$Na_xV_2O_5$ ($x = 0.33$), in which the majority of the donated 0.33 electrons occupy the vanadium position at V_1 sites and the other fraction at V_3 sites (8). However, Hirshinger *et al.* (9) recently reported a study of β-$Li_xV_2O_5$ by ^6Li and ^7Li NMR, which showed that the unpaired electrons would be localized equally in V_1, V_2, and V_3 sites. Vanadium ions are found in both V^{4+} and V^{5+} states and the structure is composed of V^{4+}–V^{4+} dimers (4, 10, 11), which have a spin singlet ground state $S = 0$ and a triplet state $S = 1$ for the first excited state, as described by the bipolaron model of Chakraverty *et al.* (11). The triple state is not thermally accessible because the bipolaron dissociates into two polarons ($S = 1/2$) with a dissociation energy 2Δ which is smaller than the single–triplet exchange energy $2J$ (Fig. 2). Magnetic susceptibility measurements allow one to determine the unpaired electron population and the dissociation energy 2Δ. The same information, in addition to the interaction between electron spins and the hyperfine interaction with ^{51}V nuclei, can also be obtained by EPR measurements.

EPR and magnetic susceptibility measurements have shown that the bipolaron model describes accurately the electronic properties of the sol–gel β-$Na_{0.33}V_2O_5$ compound with parameters of the same order as for the classical compound (4). The electronic properties are thus independent of the synthesis procedure, and the difference between the electrochemical properties could be due rather to different electronic behavior during the lithium electrochemical insertion into the initial compound. It would be necessary to study the electronic properties of $Li_xNa_{0.33}V_2O_5$ samples ($0 < x < 1.66$) where Li is electrochemically inserted. However, the determination

0022-4596/95 $12.00

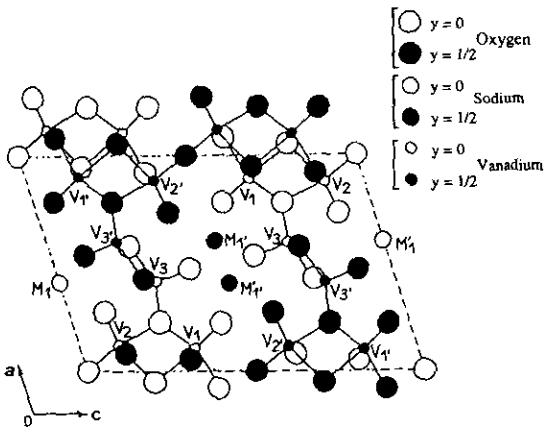

FIG. 1. Projection in the (a, c) plane of the atomic positions in the monoclinic $Na_{0.33}V_2O_5$ bronze, after Refs. (5–7).

of the electronic behavior of mixed $Li_xNa_yV_2O_5$ ($0.23 \leq x + y \leq 0.37$) compounds with β-monoclinic structure is fundamental for understanding the influence of the initial presence of Li ions in M_I and M_I' tunnel sites on the electronic properties.

The existence domain of monoclinic $M_xV_2O_5$ phase is $0.22 \leq x \leq 0.4$ and $0.22 \leq x \leq 0.62$ for M = Na and M = Li (12), respectively. In the case of $Li_xV_2O_5$, Galy *et al.* (6) have shown that the monoclinic domain can be decomposed in two domains which can be attributed, respectively, to β-phase ($0.22 \leq x \leq 0.37$) and β′-phase ($0.44 \leq x \leq 0.49$), which has a structure very close to β-phase. It is possible to prepare mixed (Li, Na) vanadium bronzes with a β-monoclinic structure up to Li composition x equal to 0.23 per mole V_2O_5 by the sol–gel process. These particular materials have never been synthesized by solid state reaction. The compounds $Li_xNa_yV_2O_5$ have always been synthesized at room temperature, either by electrochemical insertion of Li in $Na_yV_2O_5$ (x = 0.25 and 0.40) (13) or by chemical insertion of Li in $Na_yV_2O_5$ with LiI (14). However, in neither case, have their electronic properties been studied.

Our purpose is to describe the sol–gel synthesis of β-monoclinic $(Li_xNa_y)V_2O_5$ bronzes with $0.23 \leq x + y \leq 0.37$, and to deduce some of their electronic properties from EPR, magnetic susceptibility, and electrical conductivity measurements.

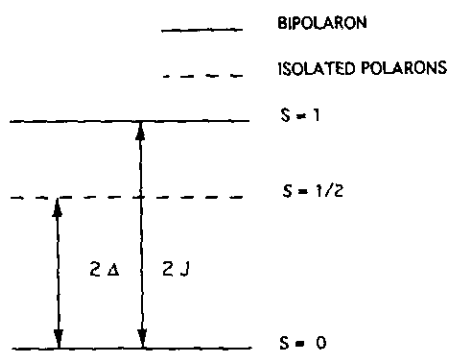

FIG. 2. Schematic representation of the two lowest spin states of bipolarons and of the isolated polaron state. 2J and 2Δ are, respectively, the singlet–triplet exchange energy and the dissociated energy of the bipolaron.

EXPERIMENTAL

Chemical analysis of compounds has been performed by oxidation–reduction to determine the V^{4+}/V_{total} content, and by atomic absorption measurements (Varian, Model AA-275) to determine the amount of Li^+ and Na^+ cations. X-ray diffraction experiments have been performed using a reflection geometry diffractometer (λ Cu $K\alpha$ wavelength = 1.5418 Å). Magnetic susceptibility measurements were performed with a Faraday electrobalance in the temperature range 4 to 300 K. EPR spectra were recorded between 4 and 300 K on a Bruker 220D spectrometer operating at X-band and equipped with an ESR9 helium flow cryostat (Oxford Instrument). The magnetic field and the microwave frequency were measured, respectively, with a Gaussmeter and frequency meter. Direct-current conductivity measurements were performed at temperatures between 40 and 300 K on bronze films parallel and perpendicular to their surfaces. Silver electrodes were deposited on the film in order to ensure contact resistance. The dc current passing through the sample from a Keithley constant-current source was kept at about 0.1 μA and the applied voltage on the film was measured with a Keithley voltmeter. Impedance and dielectric relaxation measurements (15) were performed only on $Li_{0.23}V_2O_5$ in the temperature range 240–300 K, under dry N_2 flux, in a broad frequency range 10 Hz–10 GHz using HP 8751 and 8510 network analyzers. The cell is an APC7 circular coaxial line whose inner conductor is interrupted by a cylindrically oriented sample pellet, which is made up of several superposed pieces of film heat treated at about 560°C. The applied electric field is parallel to the pellet axis, i.e., perpendicular to the constitutive films. The experimental setup was described elsewhere (16).

SYNTHESIS OF $Li_xNa_yV_2O_5$ BRONZES BY A SOL–GEL PROCESS

The synthesis of bronzes by a sol-gel process includes three steps:

(a) The first step is the synthesis of V_2O_5 gels by acidification of a sodium metavanadate solution by passing it through an ion exchange resin (17). The resulting gel exhibits an entangled fibrous structure, resembling flat

ribbons about 10 Å thick (18). The ribbons have a structure close to that of orthorhombic V_2O_5 (19). By spreading the gel on a plane surface, the ribbons set nearly parallel to it and X-ray reflection geometry diagrams show a series of $00l$ peaks of 1D order perpendicular to the platelet: the d-spacing is about 11.6 Å, corresponding to one interfoliar water layer (2.8 Å thick). The ribbons are negatively charged, with about 0.4 charge per V_2O_5; this charge is compensated for by 0.4 H_3O^+ ions leading thus to ionic exchange properties between the H_3O^+ cations and other charged species, as for example, M^{z+} cations.

(b) The second step is the synthesis of $Li_xNa_yV_2O_5 \cdot nH_2O$ xerogels by ionic exchange. The preparation procedure is carried out in such a way that the initial anisotropy of the xerogel during the intercalation reaction is preserved: the gel is spread as a thin layer over a glass plate. Simultaneous intercalation of Li^+ and Na^+ ions is obtained by the direct immersion of the xerogel film in a chloride solution containing either the Li^+ ion in the case of $Li_xV_2O_5 \cdot nH_2O$ or the two ions in the case of $Li_xNa_yV_2O_5 \cdot nH_2O$. The intercalation reaction is achieved after about 20 min, by using solutions corresponding to the following salt concentrations: NaCl (0.04 *M*)/LiCl (0.06 *M*); NaCl (0.02 *M*)/LiCl (0.08 *M*); NaCl (0.01 *M*)/LiCl (0.09 *M*); and LiCl (0.1 *M*). The number of intercalated cations depends on their hydration number which is equal to 6 H_2O for Li^+ and 4 H_2O for Na^+ (20) and on the duration of the exchange. In both compounds, $Li_xV_2O_5$ and $Na_yV_2O_5$, the exchange is completely achieved after 30 min. As the hydrated ion is larger in the case of Li^+ than in the case of Na^+, the maximum amount of cation that is possible to intercalate into the xerogel is lower for Li^+ (0.23) than for Na^+ (0.33). The total amount of water determined by thermal analysis is about 1.55 H_2O moles/V_2O_5. The d-spacing between the xerogel ribbons is dependent on the nature of the intercalated ions: from 10.91 Å for Na^+ ions to 11.24 Å for Li^+ ions (Table 1).

(c) The last step is the preparation of vanadium bronzes $Li_xNa_yV_2O_5$. These compounds are prepared by heat treatment of intercalated xerogels, which gives a black sample with a slight metallic reflection. From DTA and GTA analysis, we may consider that the transformation of the intercalated xerogels into bronzes is achieved at 550°C. It has already been shown (21) that the formation of these bronzes is due to an oxidation–reduction reaction via the two systems V^{5+}/V^{4+} and OH^-/O_2. The compounds have been chemically analyzed by atomic absorption measurements to determine the (Na, Li) content and by oxidation–reduction measurements to determine the ratio V^{4+}/V_{total}. X-ray diffraction performed on intercalated xerogel thin layers show that all the compounds are monoclinic. The parameters a, b, and β are nearly constant, and the c parameter increases with the lithium content (cf. Table 2). As in the case of $Na_{0.33}V_2O_5$ bronze (4), only the Bragg peaks 002, 004, 104, and 106 appear with noticeable intensities on diffraction patterns in reflection geometry (Fig. 3). This feature indicates that the film plane P containing the b axis has a normal n whose average direction deviates from the c and a axes by $\phi \approx 4.6°$ and $(\beta + \phi) \approx 114.6°$, respectively (Fig. 4). This preferred orientation is also confirmed by SEM experiments performed on $Li_{0.23}Na_{0.14}V_2O_5$ sol–gel bronze surface, showing slabs of about 10 × 1 μm elongated in the film plane (Fig. 5).

TABLE 2
Structural Parameters of the Monoclinic Bronzes

Parameters	a(Å)	b(Å)	c(Å)	β(°)
$Na_{0.33}V_2O_5$	10.10 ± 0.04	3.62 ± 0.02	15.15 ± 0.05	110.0 ± 0.1
$Li_{0.11}Na_{0.23}V_2O_5$	10.00 ± 0.04	3.60 ± 0.02	15.20 ± 0.05	109.0 ± 0.1
$Li_{0.23}Na_{0.14}V_2O_5$	10.04 ± 0.04	3.60 ± 0.02	15.22 ± 0.05	109.9 ± 0.1
$Li_{0.23}V_2O_5$	10.03 ± 0.04	3.60 ± 0.02	15.38 ± 0.05	110.7 ± 0.1

RESULTS AND DISCUSSION

Magnetic Susceptibility Measurements

In the case of the bronze β-$Na_{0.33}V_2O_5$, it was previously shown (4, 10) that it is possible to distinguish:

TABLE 1
Characteristic Data of Xerogels

	Concentration of exchange solutions				
	NaCl 0.1 *M* —	NaCl 0.04 *M* LiCl 0.06 *M*	NaCl 0.02 *M* LiCl 0.08 *M*	NaCl 0.01 *M* LiCl 0.09 *M*	— LiCl 0.1 *M*
Xerogel formula	$Na_{0.33}V_2O_5$ 1.6 H_2O	$Li_{0.11}Na_{0.23}$ V_2O_5 1.55 H_2O	$Li_{0.23}Na_{0.14}$ V_2O_5 1.55 H_2O	$Li_{0.23}Na_{0.07}$ V_2O_5 1.55 H_2O	$Li_{0.23}V_2O_5$ 1.55 H_2O
d-Spacing (Å) (±0.05 Å)	10.91	10.95	11.03	11.21	11.24

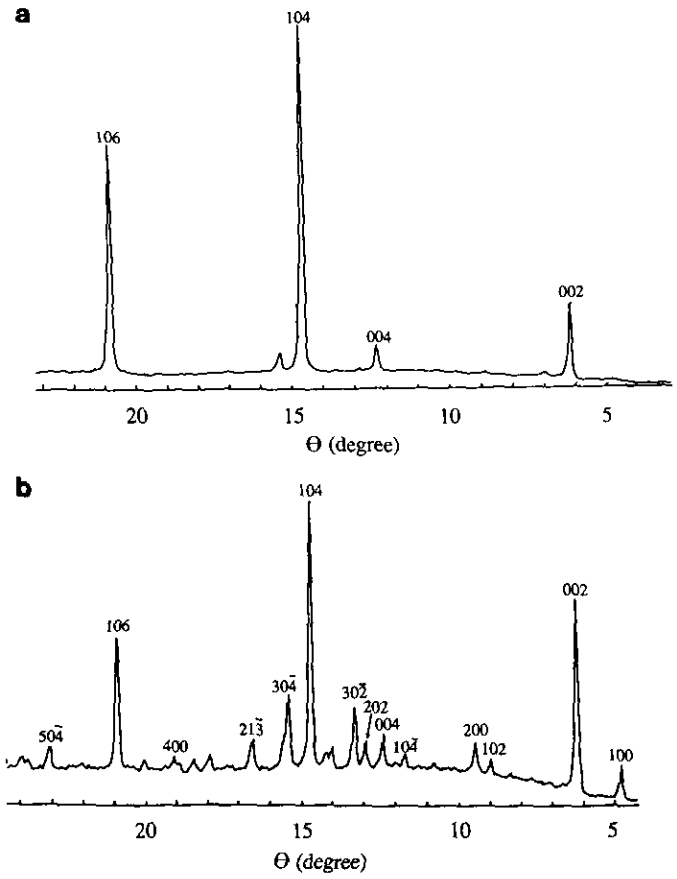

FIG. 3. X-ray diffraction spectra (reflection geometry, $\lambda_{CuK\alpha}$) of $Li_{0.23}Na_{0.14}V_2O_5$ bronze (a) film and (b) powder.

(i) the polarons at V_1 sites of the β-monoclinic structure resulting from the thermal dissociation of singlet bipolarons whose susceptibility is given by the expression

$$\chi_1 = (C_1/T) \cdot \exp(-\Delta/kT)/[1 + \exp(-\Delta/kT)], \quad [1]$$

where C_1 is the Curie constant and 2Δ is the dissociation energy of the bipolaron; and

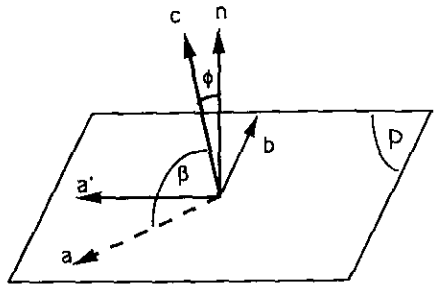

FIG. 4. Schematic representation of the orientation of the film plane P of the bronze with respect to the crystallographic axes of the monoclinic structure; (*a'*) orthogonal projection of *a* axis on the film plane P; (*n*) normal to the film plane P.

(ii) isolated polarons, whose number is independent of temperature, so that their magnetic susceptibility χ_2 follows a simple Curie–Weiss law

$$\chi_2 = C_2/(T + \Theta_p), \quad [2]$$

where C_2 and Θ_p are, respectively, the Curie constant and the Curie temperature.

Consequently, the total susceptibility associated to polarons can be expressed as:

$$\chi = \chi_1 + \chi_2. \quad [3]$$

At very low temperatures ($T \approx 4$ K), all the bipolarons are in the singlet state ($S = 0$) and are not dissociated. The susceptibility χ is thus due to isolated polarons, i.e., $\chi \approx \chi_2$.

Magnetic measurements have been performed on three compounds: $Li_{0.23}V_2O_5$, $Li_{0.23}Na_{0.14}V_2O_5$, and $Li_{0.11}Na_{0.23}V_2O_5$. A typical temperature dependence of χ is shown in Fig. 6. The magnetic susceptibility follows a Curie–Weiss behavior, due to isolated polarons, for $T <$ 25 K. Consequently, the deviation from the Curie–Weiss law at higher temperatures is due to the contribution of the dissociated bipolarons. It is thus possible to determine the different parameters C_1, C_2, Θ_p, and Δ by fitting the experimental results to expressions [1] to [3]. The results obtained for the three bronzes are summarized in Table 3. The proportions of isolated polarons (p_2) and polarons resulting from the thermal dissociation of the bipolarons (p_1) are expressed as: $p_1 = C_1/(C_1 + C_2)$ and $p_2 = C_2/(C_1 + C_2)$. The results are given in Table 4. Table 3 shows that the values of C_1, C_2, Θ_p, and Δ are very similar for all the compounds, except for the dissociation energy of $Li_{0.23}V_2O_5$, which is larger than that of sodium and mixed compounds.

EPR Measurements

EPR spectroscopy allows the detection of isolated polarons ($S = 1/2$). The bipolaron triplet state ($S = 1$) should give rise to a characteristic EPR spectrum, but

TABLE 3
Parameters Deduced from Magnetic Susceptibility Measurements

Compounds	C_1 (emuK/mole)	C_2 (emuK/mole)	Θ_p (K)	Δ (eV)
$Na_{0.33}V_2O_5$[a]	0.223	0.042	20	1.45×10^{-2}
$Li_{0.11}Na_{0.23}V_2O_5$	0.121	0.060	33	1.18×10^{-2}
$Li_{0.23}Na_{0.14}V_2O_5$	0.128	0.045	19.5	0.95×10^{-2}
$Li_{0.23}V_2O_5$	0.215	0.051	6	3×10^{-2}

[a] From Ref. (4).

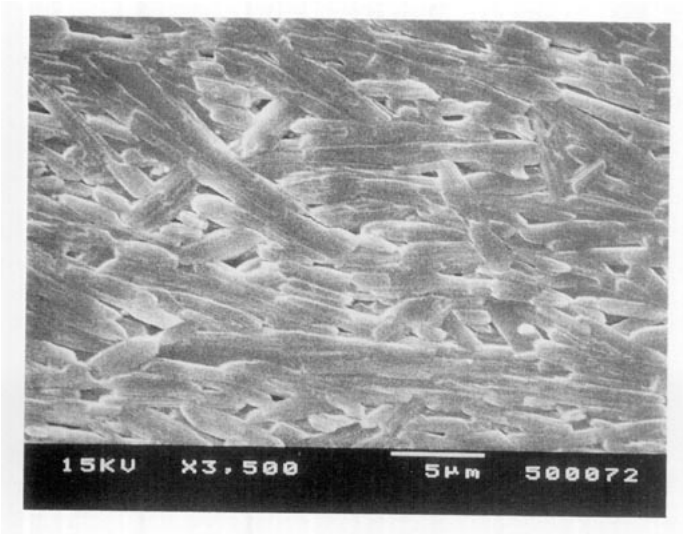

FIG. 5. SEM micrographs of the surface of $Li_xNa_yV_2O_5$ bronze film.

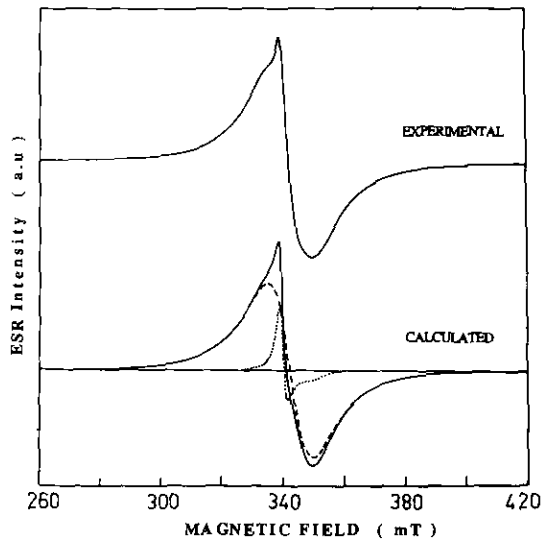

FIG. 7. EPR spectrum at 110 K of $Li_{0.23}Na_{0.14}V_2O_5$ bronze film recorded with magnetic field B parallel to the film plane. Microwave frequency 9434.26 MHz. This spectrum is simulated by the sum of two different components: a broad Lorentzian line at $g = 1.950$ and linewidth $\Delta B = 11.5$ mT, and an anisotropic signal with powder-like lineshape characterized by the following parameters $g_\parallel = 1.982$, $g_\perp = 1.934$, $\Delta B_\parallel = 2$ mT, $\Delta B_\perp = 6$ mT.

this state is not thermally accessible since the dissociation energy 2Δ of the bipolaron is lower than the singlet–triplet exchange energy $2J$. Figure 7 shows the EPR spectrum of sol–gel bronze films of composition $Li_{0.23}Na_{0.14}V_2O_5$ with the magnetic field perpendicular to the film plane ($\theta = 0$). This spectrum is accurately simulated by the sum of two different components: a broad isotropic line with a g factor equal to 1.950 and a narrow anisotropic powder-like line with $g_\parallel = 1.982$ and $g_\perp = 1.934$. All the other bronze compositions exhibit the same EPR lineshape, and only the ratio of the "narrow" to the "broad" components is composition dependent. The contribution of the narrow spectrum increases with the lithium content: 0% in $Na_{0.33}V_2O_5$, up to 6% in $Li_{0.23}V_2O_5$ and about 4% for $Li_xNa_yV_2O_5$. As described in Ref. (4) for the sol–gel bronze $Na_{0.33}V_2O_5$, the broad line corresponds to the beta-monoclinic phase (β-phase). There are two possible origins for the narrow component: (i) the gamma-orthorhombic phase of the lithium vanadium bronze (γ-phase), which gives a very similar EPR spectrum, as described in a forthcoming paper (22); or (ii) a $Li_{1+x}V_3O_8$ phase, which has, however, never been identified by EPR measurements and which is represented on the XRD spectrum of $Li_xNa_yV_2O_5$ ($x \neq 0$) by a weak peak. From the phase diagram of $Li_xV_2O_5$, the γ-phase appears during the cooling process for $x \geq 0.5$, because of small inhomogeneities in the lithium concentration. As the proportion of this narrow line in the compound has been evaluated to few percent (<6%), we considered only the intense line corresponding to the β-phase. The EPR spectrum of sol–gel bronze films with composition $Li_{0.23}Na_{0.14}V_2O_5$, recorded with the magnetic field parallel to the film plane ($\theta = \pi/2$), has been simulated and the g factor obtained for the β-phase is 1.975. So, it is possible to estimate the g powder factor with the relation

$$g_{\text{powder}} \approx (2g_\perp + g_\parallel)/3. \qquad [4]$$

The values of different parameters $g_\parallel$, $g_\perp$, $\Delta B_\parallel$, $\Delta B_\perp$ are given in Table 5. If we consider the linewidths of $\Delta B_\parallel$ and $\Delta B_\perp$ at 110 K, it appears that they increase with increasing Na content for the different compounds, except for $Li_{0.23}V_2O_5$.

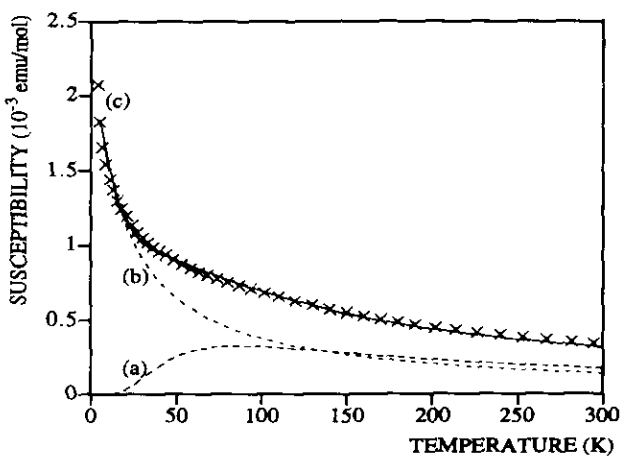

FIG. 6. The experimental temperature dependence of the magnetic susceptibility of $Li_{0.23}Na_{0.14}V_2O_5$ bronze (crosses) is due to: (a) polarons at the V_1 site resulting from the thermal dissociation of bipolarons; (b) isolated polarons at V_1 and V_3 sites (dashed lines). The full line represents the sum of these two contributions.

TABLE 4
Polarons Populations, p_1 and p_2, and Bipolaron Dissociation Energy Obtained by EPR and Magnetic Susceptibility

Compounds	p_1 Dissociated bipolarons (%)	p_2 Isolated polarons (%)	Δ(eV)	p_1 Dissociated bipolarons (%)	p_2 Isolated polarons (%)	Δ(eV)
$Na_{0.33}V_2O_5$[a]	82	18	1.45×10^{-2}	84	16	1.45×10^{-2}
$Li_{0.11}Na_{0.23}V_2O_5$	70	30	1.34×10^{-2}	67	33	1.18×10^{-2}
$Li_{0.23}Na_{0.14}V_2O_5$	77	23	1.22×10^{-2}	74	26	0.95×10^{-2}
$Li_{0.23}V_2O_5$	72	28	3×10^{-2}	80	20	3×10^{-2}

[a] From Ref. (4).

Figure 8 shows the variation of the peak-to-peak linewidth ΔB at 25 and 110 K for different orientations θ of the bronze $Li_{0.23}Na_{0.14}V_2O_5$ film surface with respect to the magnetic field B (θ being the angle between B and the normal to the film). This type of variation has roughly a sinusoidal shape of period π. The amplitude of this variation decreases with increasing temperature. Consequently, the anisotropy of the dipolar spin–spin interactions, which governs the linewidth, is higher at low temperature. At high temperature, where the polaron motion becomes important, these interactions are submitted to a motionally averaged dipolar interaction: the resulting linewidth becomes nearly independent of the angle θ. In contrast, as the temperature decreases, the polaron motion is slowed, which results in an increase in dipolar spin–spin interactions.

Figure 9 shows an example of the temperature dependence of the EPR linewidth ΔB, in which it is possible to distinguish two regimes: (i) at low temperature ($T < 50$ K), the linewidth is nearly temperature independent; (ii) at high temperature ($T > 50$ K), the linewidth increases with temperature. To a first approximation, the EPR linewidth is essentially due to dipolar interactions between polarons. It is proportional to $1/\langle R^3 \rangle$, where R is the distance between polarons. Consequently, the EPR linewidth can be considered as proportional to the polaron concentration

$$\Delta B = a + b \exp(-\Delta/kT)/[1 + \exp(-\Delta/kT)], \quad [5]$$

TABLE 5
Characteristic Parameters of EPR Spectra

Compounds	$g_\parallel$	$\Delta B_\parallel$(mT)[a]	$g_\perp$	$\Delta B_\perp$(mT)[a]
$Na_{0.33}V_2O_5$[b]	1.940	15.8	1.976	17.1
$Li_{0.11}Na_{0.23}V_2O_5$	1.940	14.3	1.975	15.4
$Li_{0.23}Na_{0.14}V_2O_5$	1.950	10.0	1.975	13.6
$Li_{0.23}V_2O_5$	1.940	11.5	1.975	14.5

[a] Measured at 110 K.
[b] From Ref. (4).

where a and b are constants, 2Δ being the dissociation energy of the bipolarons. Below 50 K, all the bipolarons are in the singlet state and thus only the isolated polarons contribute to the EPR spectrum. Since the concentration of these polarons does not vary with temperature, the average distance $\langle R \rangle$ between polarons and hence the EPR linewidth are constant below 50 K, i.e., $\Delta B \approx a$. At higher temperature, the increase in the polaron concentration due to the dissociation of bipolarons gives rise to an increase in the EPR linewidth ΔB, as described by expression [5] in which b and Δ parameters are adjusted to obtain the best fit to the experimental results (cf. Table 6). From a and b values, it is possible to obtain the proportions p_2 and p_1 of isolated and associated polarons, respectively, $p_2 = a/(a + b)$ and $p_1 = b/(a + b)$. The results are shown in Table 4. The values of the dissociation energies Δ and of the populations p_2 and p_1, measured from EPR linewidths and magnetic susceptibility, are in good agreement. The fact that these two independent methods give very similar results is an important argument in favor of the bipolaron model. The values of p_1 and p_2 do not significantly depend on the Li and Na content of the bronze. The dissociation energy of the

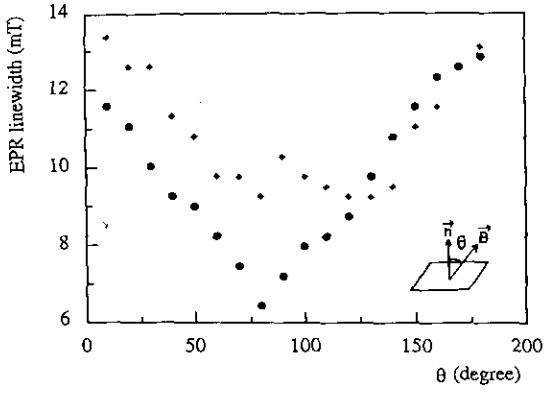

FIG. 8. Variation of the EPR linewidth with the angle between the magnetic field and the direction perpendicular to the film plane for the bronze $Li_{0.23}Na_{0.14}V_2O_5$. Circles, $T = 25$ K; diamonds, $T = 110$ K.

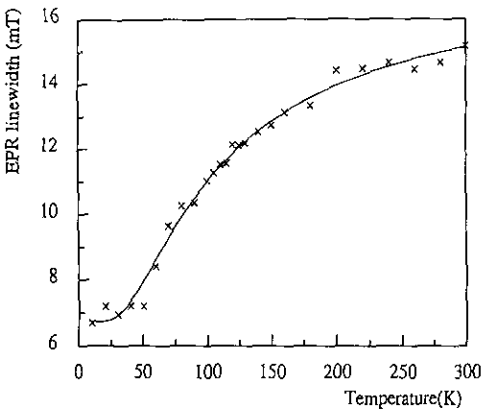

FIG. 9. Temperature dependence of the EPR linewidth of $Li_{0.23}Na_{0.14}V_2O_5$ bronze film when the magnetic film B is parallel to the film plane. The solid line represents the variation calculated using expression [4] with $a = 6.7$ mT and $b = 21.9$ mT.

bipolarons, determined either by EPR linewidth or by magnetic susceptibility, increases with the sodium content, except for the case of the bronze $Li_{0.23}V_2O_5$.

The population p_2 of isolated polarons ranges between 16 and 33%. Hirschinger *et al.* (9) showed by NMR that the unpaired electrons in β-phase are equally distributed among the three sites V_1, V_2, and V_3. Thus, a population p_2 of 16 to 33% of V^{4+} ions which do not form dimers at low temperature could correspond to the trigonal bipyramid V_3 site, while the bipolarons could be due to V^{4+} ions in edge-sharing octahedral V_1 and V_2 sites.

Conductivity Measurements

As described in previous papers (4, 23, 24), the conductivity of the monoclinic bronzes contains two contributions: (i) a component σ_b, due to electron hopping (bipolaron and polaron motion) along zigzag chains of vanadium ions (V_1 sites) parallel to the b direction and (ii) a component σ_a, due to electron hopping (polaron motion) along the sequence $V_1V_3V_3'V_1'V_1 \ldots$ parallel to the a direction (Fig. 1).

TABLE 6
Parameters Deduced from EPR Measurements

Compounds	a(G)	b(G)	Δ(eV)
$Na_{0.33}V_2O_5$[a] film$\parallel$ to B	90	406	1.45×10^{-2}
$Li_{0.11}Na_{0.23}V_2O_5$ film$\parallel$ to B	99	229	1.34×10^{-2}
$Li_{0.23}Na_{0.14}V_2O_5$ film$\parallel$ to B	67	219	1.22×10^{-2}
$Li_{0.23}V_2O_5$ powder	107	272	3×10^{-2}

[a] From Ref. (4).

The conductivity of the bronzes can be described by the expression (24, 25)

$$\sigma_{a,b} = N_{a,b}e^2l_{a,b}^2/(kT\tau_c) \cdot \exp(-W_{a,b}/kT), \qquad [6]$$

where $\sigma_{a,b}$ is the conductivity parallel to a or b with corresponding hopping distance $l_{a,b}$ ($l_a \approx 10$ Å; $l_b \approx 3.6$ Å) and activation energy $W_{a,b}$, where τ_c is the correlation time of electron hopping from V_1 to V_1 or V_1 to V_3 sites (23, 24) (Fig. 1). $N_{a,b}$ is the number of electrons per unit volume involved in the conductivity parallel to a or b. N_a is expressed as

$$N_a = N_0(x + y)/2 \cdot [p_2 + p_1 \exp(-\Delta/kT)/(1 + \exp(-\Delta/kT))], \qquad [7]$$

where N_0 is the number of vanadium ions. The parameters p_1, p_2, and Δ are those determined by EPR and susceptibility measurements. Conductivities of the sol–gel bronzes $Li_{0.23}V_2O_5$ and $Li_xNa_yV_2O_5$ have been measured parallel ($\sigma_\parallel$) and perpendicular ($\sigma_\perp$) to the film plane (P). Consequently, $\sigma_\parallel$ is an average value of the conductivities σ_b and $\sigma_{a'}$, parallel, respectively, to b and a' axes (the a' axis being the orthogonal projection of the a axis on the film plane (Fig. 4)), i.e., $\sigma_\parallel = (\sigma_b + \sigma_{a'})/2$. The hopping distance along this direction is $l_{a'} = l_a \cdot |\sin(\beta + \phi)|$. It results from expression [6] that $\sigma_{a'} = \sigma_a \cdot \sin^2(\beta + \phi)$ and $\sigma_\parallel = [\sigma_b + \sigma_a \cdot \sin^2(\beta + \phi)]/2$. Moreover, as the hopping distance l_n parallel to the direction n (normal to the film) corresponds to the orthogonal projection of the hopping distance l_a on n, i.e., $l_n = l_a \cdot |\cos(\beta + \phi)|$, thus $\sigma_\perp = \sigma_a \cdot \cos^2(\beta + \phi)$. Since the angle $(\beta + \phi)$ is equal to 114.6°, it follows that:

$$\sigma_\parallel = [\sigma_b + 0.83\ \sigma_a]/2 \text{ and } \sigma_\perp = 0.17\ \sigma_a. \qquad [8]$$

However, as shown in SEM experiments (Fig. 5), the bronze films are porous and composed of crystalline slabs. Consequently, the conductivity values (hereafter referred to as $\sigma_{f\parallel}$ and $\sigma_{f\perp}$ measured by direct-current technique are undervalued with respect to their exact values, since they are limited by contact resistances and capacitances between the slabs. In this way, alternating current techniques at frequencies lower than 50 MHz appear more suitable to demonstrate the slab boundaries phenomena and determine the actual bronze (or slab) conductivities $\sigma_\parallel$ and $\sigma_\perp$ in order to calculate σ_a and σ_b from Eq. [8]. Nevertheless, the dc technique has the advantage of giving measurements in a broad temperature range, contrary to the ac-technique, which involves a coaxial cell accurately calibrated only for temperatures between 200 and 300 K. Moreover, the conductivity measured by the dc technique has the same temperature dependence as the conductivity obtained by the ac tech-

nique since they are proportional, as specified further in this paper.

(*a*) *Direct-current conductivity measurements.* The temperature dependence, given by $\log \sigma T = f(1/T)$, of the conductivities $\sigma_{f\parallel}$ and $\sigma_{f\perp}$ of the films are shown in Fig. 10 (see also Table 7). It can be observed that the latter exhibit an anisotropic conductivity described by the ratio $R = \sigma_{f\parallel}/\sigma_{f\perp}$, which is maximum for the mixed bronzes ($R \approx 1000$ at room temperature) and minimum for $Li_{0.23}V_2O_5$ ($R \approx 20$ at room temperature). The evolution of $\sigma_{f\parallel}$ and $\sigma_{f\perp}$ versus T shows three different regimes:

(i) the "high temperature" domain I above 100 K, where $\sigma_{f\parallel}$ and $\sigma_{f\perp}$ follow the Arrhenius law with activation energies varying from 0.11 to 0.07 eV with the sodium content (Table 7);

(ii) the "intermediate temperature" domain II ($40 < T < 100$ K), where the activation energies decrease while cooling; and

(iii) the "low temperature" domain III, where the conductivity increases sharply near 40 K when the temperature decreases in the case of mixed and lithium bronzes.

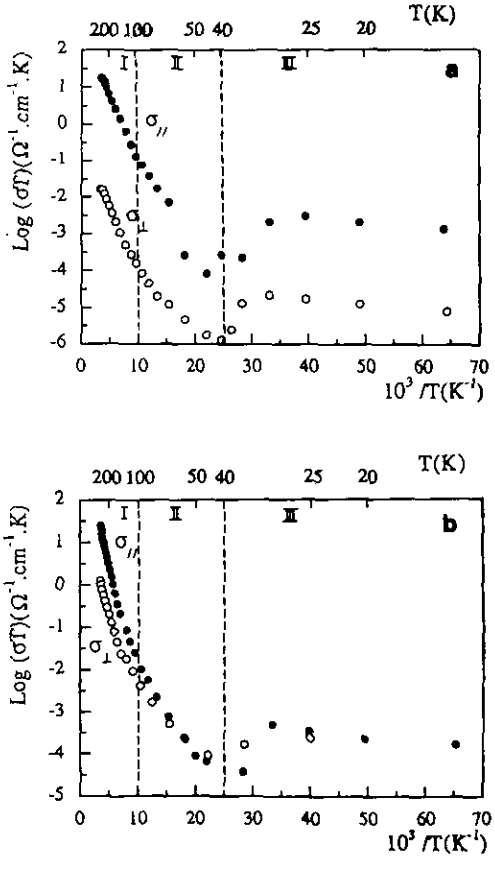

FIG. 10. Inverse temperature dependence of the dc-electrical conductivity, $\log(\sigma_f T) = f(10^3/T)$ for: (a) $Li_{0.11}Na_{0.23}V_2O_5$ and (b) $Li_{0.23}V_2O_5$. $\sigma_{f\parallel}$ (solid circles) and $\sigma_{f\perp}$ (open circles) represent, respectively, the conductivities parallel and perpendicular to the film plane.

TABLE 7
Conductivities and Activation Energies Obtained by dc Conductivity Measurements on Bronze Films

Compounds	$\sigma_{f\parallel}$(S · cm^{-1})	$W_\parallel$(eV)	$\sigma_{f\perp}$(S · cm^{-1})	$W_\perp$(eV)	$\sigma_{f\parallel}/\sigma_{f\perp}$
$Na_{0.33}V_2O_5$[a]	8	0.07	4×10^{-2}	0.07	200
$Li_{0.11}Na_{0.23}V_2O_5$	5.98×10^{-2}	0.08	5.48×10^{-5}	0.07	1091
$Li_{0.23}Na_{0.14}V_2O_5$	0.138	0.09	1.08×10^{-4}	0.08	1278
$Li_{0.23}V_2O_5$	8.6×10^{-2}	0.11	4.3×10^{-3}	0.11	20

[a] From Ref. (4).

Below 30 K, the conductivity decreases with temperature.

In the high temperature domain I, all phonon spectra take place in an activated hopping of the electrons above $\Theta_D/2$, where $\Theta_D/2 \approx 200$ K is the Debye temperature for the mixed and lithium bronzes. The anisotropy factors R are constant in this temperature domain.

Below $\Theta_D/2$, the phonon spectra freezes progressively, which gives rise to a progressive decrease in activation energy. In the low temperature domain ($T \leq 40$ K), the anomaly of the conductivity behavior could be explained by the existence of a structural phase transition at 40 K. The anisotropy factor R decreases from 1000 to 100 for mixed bronzes and from 20 to 1 for lithium bronze below 100 K.

The three different conductivity regimes correspond to the magnetic properties (susceptibility and EPR linewidths) of the material. In particular, the low temperature regime III, below 40 K, corresponds to the existence of undissociated bipolarons coexisting with isolated polarons at V_3 sites. The high temperature regimes I and II correspond to the rapid thermal dissociation of bipolarons into polarons.

(*b*) *Alternating-current conductivity measurements.* Ac-conductivity and permittivity measurements between 10 Hz and 10 GHz, which will be fully described in a forthcoming paper (15) for $Li_{0.23}V_2O_5$ bronze allow one to obtain the slab conductivity $\sigma_\perp$ and to demonstrate a dielectric relaxation due to electron hopping along the sequence $V_1V_3V_{3'}V_{1'}$ (Fig. 1), whose characteristic correlation time is τ_c. The measured correlation time $\tau_c \approx 3.3 \times 10^{-12}$ sec (15) is on the same order of magnitude as that found in sodium (β-$Na_{0.33}V_2O_5$) (16) and silver (β-$Ag_{0.3}V_2O_5$) (25) monoclinic bronzes, i.e., $\tau_c \approx 10^{-11}$ sec.

The slab conductivity of $Li_{0.23}V_2O_5$ has been obtained by the complex impedance method in the low-frequency domain. Figure 11 shows a typical complex resistivity diagram, $\rho'' = f(\rho')$, at room temperature. The resistivity ρ is proportional to the impedance Z by the expression $Z = \rho l/S$, where l and S are, respectively, sample thickness and area. The deconvolution of this plot reveals two circular arcs corresponding to a series combination of

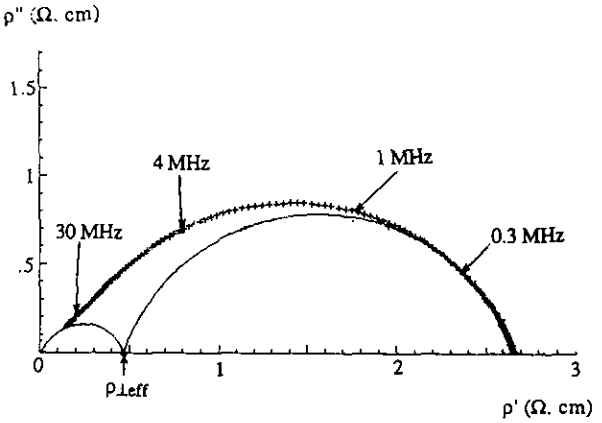

FIG. 11. Complex resistivity plots (ρ'' vs ρ') for $Li_{0.23}V_2O_5$ at 296 K perpendicular to the the film plane.

two impedance (resistivity) relaxations, which are each associated with a parallel combination of a resistance and capacitance (Fig. 11): the first is due to contact resistance and capacitance between the crystalline slab and the second to the resistance and capacitance of the slabs. The common intersection of the two circles with the real ρ' axis allows one to obtain the slab dc-resistivity $\rho_\perp$. It follows that the slab conductivity $\sigma_\perp = 1/\rho_\perp$ is higher than the film conductivity $\sigma_{f\perp}$ measured by the dc technique, i.e., $\sigma_\perp = 2.1 \times 10^{-2}$ S · cm^{-1} and $\sigma_{f\perp} \approx 4 \times 10^{-3}$ S · cm^{-1} at room temperature. These two parameters have approximatively the same activation energy, i.e., $W \approx 0.1$ eV. However, the conductivity $\sigma_\perp$ is that of an effective medium (hereafter denoted $\sigma_{\perp\text{eff}}$) since the films contain pores, with volume fraction $q_v \approx 0.3$. The pores are equivalent to tunnels, whose axes are perpendicular to the film plane. Since the applied electric field is parallel to the pore axis, the relation between the effective ($\sigma_{\perp\text{eff}}$) and the exact ($\sigma_\perp$) conductivity values is given by the expression:

$$\sigma_{\perp\text{eff}} = \sigma_\perp(1 - q_v). \quad [9]$$

From expressions [7], [8], and [9] and assuming the parameters $\tau_c \approx 3.3 \times 10^{-12}$ sec, $W_a = 0.11$ eV, and $\Delta = 0.03$ eV, it is found that the porous film conductivity $\sigma_{\perp\text{eff}}$ would be equal to 2.7×10^{-2} S · cm^{-1} at room temperature. This calculated value is in good agreement with the value $\sigma_{s\perp} \approx 2.2 \times 10^{-2}$ S · cm^{-1} measured on the bronze film at room temperature, within the accuracy of the measurements.

CONCLUSION

We have shown that it is possible to synthesize by sol–gel method mixed Li^+/Na^+ vanadium bronzes by double ionic exchange $H_3O^+ \rightarrow (Na^+, Li^+)$ from V_2O_5 xerogel. These compounds exhibit the same preferential orientation than monoinserted bronzes $M_xV_2O_5$ with the tunnels of the monoclinic structure parallel to the substrate.

The electronic properties of these compounds can be explained in terms of thermally dissociated bipolarons. This model explains the temperature dependences of the magnetic susceptibility and the EPR linewidth of V^{4+}. Magnetic and EPR measurements give values of the same order of magnitude for the dissociation energy 2Δ of the bipolarons and for the proportions of isolated polarons and dissociated bipolarons, i.e., 25 and 75% respectively. We have shown that all these values are very close for all the bronzes, i.e., they are almost independent of the nature of the ion in the tunnel sites of the β-monoclinic structure. Thus it seems that the initial presence of Li ions in M_I and M_I' tunnel sites does not induce notable variation of the electronic properties. However, the dissociation energy of the bipolaron is higher in the case of the compound $Li_{0.23}V_2O_5$, which contains no sodium ion. This would be probably due to a stronger electron–phonon interaction in the case of $Li_{0.23}V_2O_5$.

Dc-conductivity measurements have shown that the conductivity of the bronze films obtained by the sol–gel process is strongly anisotropic. The conductivity activation energy depends on lithium content since it ranges from 0.07 to 0.11 eV as the sodium content increases. In the case of the lithium bronze $Li_{0.23}V_2O_5$, it is shown that the film conductivity is highly dependent on the microstructure. It is thus possible to determine an exact conductivity for the bronze that agrees well with those calculated from the values of Δ and the concentration of polarons obtained by magnetic susceptibility and EPR measurements. Thus ac-conductivity measurements are under investigation for the other bronzes.

REFERENCES

1. L. Znaidi, N. Baffier, and M. Huber, *Mater. Res. Bull.* **24,** 1501 (1989).
2. J. Livage, M. Henry, and C. Sanchez, *Prog. Solid State Chem.* **18,** 259 (1988).
3. J. P. Pereira-Ramos, L. Znaidi, N. Baffier, and R. Messina, *Solid State Ionics* **28–30,** 886 (1988).
4. J. C. Badot, D. Gourier, F. Bourdeau, N. Baffier, and A. Tabuteau, *J. Solid State Chem.* **92,** 8 (1991).
5. A. D. Wadsley, *Acta Crystallogr.* **8,** 695 (1955); **10,** 261 (1957).
6. J. Galy, J. Darriet, and P. Hagenmuller, *Rev. Chem. Miner.* **8,** 509 (1971).
7. J. Galy, J. Darriet, A. Casalot, and J. B. Goodenough, *J. Solid State Chem.* **1,** 349 (1970).
8. J. B. Goodenough, *J. Solid State Chem.* **1,** 349 (1970).
9. J. Hirshinger, T. Mongrelet, C. Marichal, P. Garanger, J. M. Savariault, E. Déramond, and J. Galy, *J. Phys. Chem.* **97,** 10,301 (1993).
10. M. Onoda, T. Takahashi, and H. Nagasawa, *Phys. Status Solidi B* **109,** 793 (1982).
11. B. K. Chakraverty, M. J. Sienko, and J. Bonnerot, *Phys. Rev. B* **17,** 3781 (1978).
12. P. Hagenmuller, *in* "Non Stoichiometric Compounds, Tungsten

Bronzes, Vanadium Bronzes and Related Compounds," (D. J. Bevan and P. Hagenmuller, Eds.), Vol. 1, p. 569. Pergamon, Oxford, 1973.
13. I. D. Raistrick, *Solid State Ionics* **9,** 425 (1983).
14. M. Eguchi, Y. Muranushi, T. Miura, and T. Kishi, *Solid State Ionics* **57,** 307 (1992).
15. J. C. Badot, B. Pecquenard, and N. Baffier, unpublished results.
16. J. C. Badot and N. Baffier, *J. Solid State Chem.* **93,** 53 (1991).
17. P. Aldebert, N. Baffier, N. Gharbi, and J. Livage, *Mater. Res. Bull.* **16,** 669 (1981).
18. J. J. Legendre and J. Livage, *J. Colloid Interface Sci.* **94**(1), 75 (1983).
19. H. G. Bachman, F. R. Ahmed, and W. H. Barnes, *Z. Kristallogr.* **115,** 110 (1961).
20. N. Baffier, L. Znaidi, and J. C. Badot, *J. Chem. Soc. Faraday Trans.* **86,** 2623 (1990).
21. J. P. Pereira-Ramos, R. Messina, S. Bach, and N. Baffier, *Solid State Ionics* **40–41,** 970 (1990).
22. B. Pecquenard, D. Gourier, and N. Baffier, *Solid State Ionics,* in press.
23. H. Nagasawa and T. Erata, *J. Phys.* **43,** 1737 (1983).
24. T. Erata and H. Nagasawa, *J. Phys. Soc. Jpn.* **52,** 3652 (1983).
25. J. C. Badot, L. Binet, N. Baffier, R. Morineau, and A. Fourrier-Lamer, *Solid State Ionics* **53–56,** 343 (1992).